
GeneZip: Region-Aware Compression for Long Context DNA Modeling

Jianan Zhao^{*1,2} Xixian Liu^{*1,2} Zhihao Zhan^{1,2} Xinyu Yuan^{1,2} Hongyu Guo^{3,4} Jian Tang^{1,2,5}

Abstract

Genomic sequences span billions of base pairs (bp), posing a fundamental challenge for genome-scale foundation models. Existing approaches largely sidestep this barrier by either scaling relatively small models to long contexts or relying on heavy multi-GPU parallelism. Here we introduce GeneZip, a DNA compression model that leverages a key biological prior: genomic information is highly imbalanced—coding regions comprise only a small fraction ($\sim 2\%$) yet are information-dense, whereas most non-coding sequence is comparatively information-sparse. GeneZip couples HNet-style dynamic routing with a region-aware compression-ratio objective, enabling adaptive allocation of representation budget across genomic regions. As a result, GeneZip learns region-aware compression and achieves 137.6 \times compression with only 0.31 perplexity increase. On downstream long-context benchmarks, GeneZip achieves comparable or better performance on contact map prediction, expression quantitative trait loci prediction, and enhancer–target gene prediction. By reducing effective sequence length, GeneZip unlocks simultaneous scaling of context and capacity: compared to the prior state-of-the-art model JanusDNA, it enables training models 82.6 \times larger at 1M-bp context, supporting a 636M-parameter GeneZip model at 1M-bp context. All experiments in this paper can be trained on a single A100 80GB GPU.

1. Introduction

DNA sequence models have become central to modern genomics, enabling applications ranging from regulatory activity prediction and variant effect scoring to sequence-based modeling of three-dimensional genome organization (Avsec

et al., 2021; 2026; Fudenberg et al., 2020; Zhou, 2022; Ji et al., 2021; Zhou et al., 2024; Dalla-Torre et al., 2025; Nguyen et al., 2023; Schiff et al., 2024; Duan et al., 2025; Boshar et al., 2025). However, genome-scale settings that require contexts spanning hundreds of kilobases to megabases (Cheng et al., 2025) remain challenging because token mixing (e.g., attention (Vaswani et al., 2017)) becomes prohibitively expensive as sequence length grows.

Existing solutions largely fall into two categories. First, one can sidestep the length bottleneck by reducing model capacity (Duan et al., 2025) or relying on multi-GPU parallelism to sustain long contexts (Avsec et al., 2026), at the cost of reduced expressivity, higher hardware requirements, and increased system complexity. Second, one can convert the long-sequence problem into a shorter-sequence problem via uniform downsampling, as in Enformer and AlphaGenome, which employ U-Net-style multi-scale processing so that deeper layers operate on compressed sequences (Avsec et al., 2021; 2026).

Despite their ability to handle long inputs, these approaches share a strong implicit assumption: *all positions receive uniform representational resolution*, embracing a static downsampling schedule. This assumption is mismatched to genome biology, where information density is highly imbalanced. Protein-coding exons occupy only a small fraction of the human genome (roughly 1–2%), yet are disproportionately enriched for evolutionarily constrained positions due to purifying selection on protein function (International Human Genome Sequencing Consortium, 2001; Lindblad-Toh et al., 2011). Gene-proximal regulatory regions (e.g., promoters and other cis-regulatory elements) are also enriched for functional motifs and constraint, but are sparse and unevenly distributed across the genome (ENCODE Project Consortium, 2012; Frankish et al., 2019). By contrast, large fractions of intronic and intergenic sequence evolve under weaker constraint and often contribute limited signal for many downstream objectives (Lindblad-Toh et al., 2011). Consequently, under uniform striding or uniform compute per token, token budget is inevitably spent on low-yield regions while undersampling information-dense regions where fine-grained sequence features are most consequential.

Motivated by this imbalance, we propose GeneZip, a region-

^{*}Equal contribution. Project page: <https://github.com/AndyJZhao/GeneZip> ¹Mila - Québec AI Institute ²Université de Montréal ³National Research Council of Canada ⁴University of Ottawa ⁵HEC Montréal. Correspondence to: Jian Tang <tangjian@mila.quebec>.

adaptive compression module that learns non-uniform token allocation over ultra-long DNA. GeneZip builds on H-Net-style dynamic chunking and routing (Hwang et al., 2025) to learn content-dependent segmentation, producing compact token sequences that make expensive token mixing feasible at megabase scale. Crucially, we inject a region-aware structural prior using only static gene-structure annotations (e.g., CDS, UTR, exon, intron, promoter, and intergenic regions) (Frankish et al., 2019). During training, we supervise region-wise token budgets with a Region-Aware Ratio (RAR) loss, encouraging higher resolution in information-dense regions and stronger compression elsewhere, without using functional assay labels during compression training. We additionally introduce bounded routing to enforce global token-budget constraints, improving stability and memory predictability for long-sequence pretraining. Once trained, GeneZip can compress unseen DNA sequences without requiring annotations at inference time.

We pretrain GeneZip on the human reference genome with GENCODE-derived region annotations (Frankish et al., 2019). We show that GeneZip learns region-aware compression policies that generalize to unseen loci, achieving 137.6 base pairs per token (BPT) with only a +0.31 perplexity increase. We evaluate GeneZip on three tasks from DNALongBench (Cheng et al., 2025) and show that it is both effective and efficient. For example, on eQTL prediction, GeneZip-70M matches JanusDNA-2M (Duan et al., 2025) while delivering a $50.4\times$ speedup. All experiments in this paper can be trained on a single A100 80GB GPU.

2. Related Work

Tokenization and dynamic chunking in sequence models.

Turning raw sequential inputs into semantically meaningful and computationally efficient representations typically requires an explicit or implicit *chunking* mechanism that maps fine-grained inputs to coarser units. In language modeling, this is most commonly realized via *static* subword vocabularies learned by frequency-based algorithms such as Byte-Pair Encoding (BPE) (Sennrich et al., 2015) and SentencePiece (Kudo & Richardson, 2018), as used in large language models (Radford et al., 2019; Brown et al., 2020; Touvron et al., 2023; Grattafiori et al., 2024). In computer vision, analogous length reduction arises from spatial pooling in encoder-decoder networks (Ronneberger et al., 2015). Because these chunking rules are largely fixed, a line of tokenizer-free work models text directly at the byte level (Xue et al., 2022), introduces hierarchical multiscale compressors (Yu et al., 2023), or applies heuristic/learned boundary mechanisms such as delimiter/entropy-based chunking and token merging (Slagle, 2024; Pagnoni et al., 2024; Kallini et al., 2025). Recently, H-Net advances this direction by learning boundary decisions end-to-end and building nested hierarchies via

dynamic chunking (Hwang et al., 2025).

DNA foundation models. Large-scale self-supervised pretraining has produced transferable DNA foundation models, from k -mer/BPE Transformer encoders (DNABERT, DNABERT-2) and multi-species pretraining (Nucleotide Transformer) to long-context architectures (HyenaDNA, Caduceus, JanusDNA) (Ji et al., 2021; Zhou et al., 2024; Dalla-Torre et al., 2025; Nguyen et al., 2023; Schiff et al., 2024; Duan et al., 2025). Recently, Evo and Evo 2 have shown that scaling DNA foundation models in both taxonomic breadth (across diverse taxa) and context length improves genome-scale prediction and sequence design, thereby highlighting the importance of efficient long-range modeling (Nguyen et al., 2024; Brix et al., 2025).

Compression for long-range genomic modeling. Scaling sequence models to tens of kilobases and beyond typically requires compressing the input into a shorter latent sequence. Existing approaches largely rely on *uniform* compression, including fixed k -mer tokenization (Ji et al., 2021) and strided convolution/pooling in hierarchical encoders (often U-Net-like (Ronneberger et al., 2015)) for long-range sequence-to-function prediction (Avsec et al., 2021; 2026; Boshar et al., 2025). Uniform schemes can be mismatched to the strongly non-uniform information density of genomes: functionally important regions are sparse, e.g., protein-coding exons comprise only $\sim 1\text{--}2\%$ of the human genome yet are enriched for evolutionary constraint (International Human Genome Sequencing Consortium, 2001; Lindblad-Toh et al., 2011). Recently, several works explore learnable compression for DNA, such as vector-quantized bottlenecks (Li et al., 2024) and adaptive tokenization modules (Qiao et al., 2024), and adapts dynamic chunking ideas to genomic pretraining (Ledneva & Kuznetsov, 2025). These methods reduce sequence length either uniformly or via boundaries learned from generic objectives, but typically do not explicitly incorporate region-level biological priors into the compression policy.

GeneZip complements this line of work with two mechanisms: (i) *region-aware* compression guided by biological annotations to preserve higher resolution in information-dense regions, and (ii) *bounded routing* that enforces a predictable routing budget for robust scaling to long contexts.

3. Methodology

3.1. Problem setup and motivation

Let $x_{1:L}$ denote a DNA sequence of length L base pairs. Many long-range genomics tasks require contexts on the order of $10^5\text{--}10^6$ bp. We decompose long-range DNA modeling into three stages—encoding, token mixing, and decod-

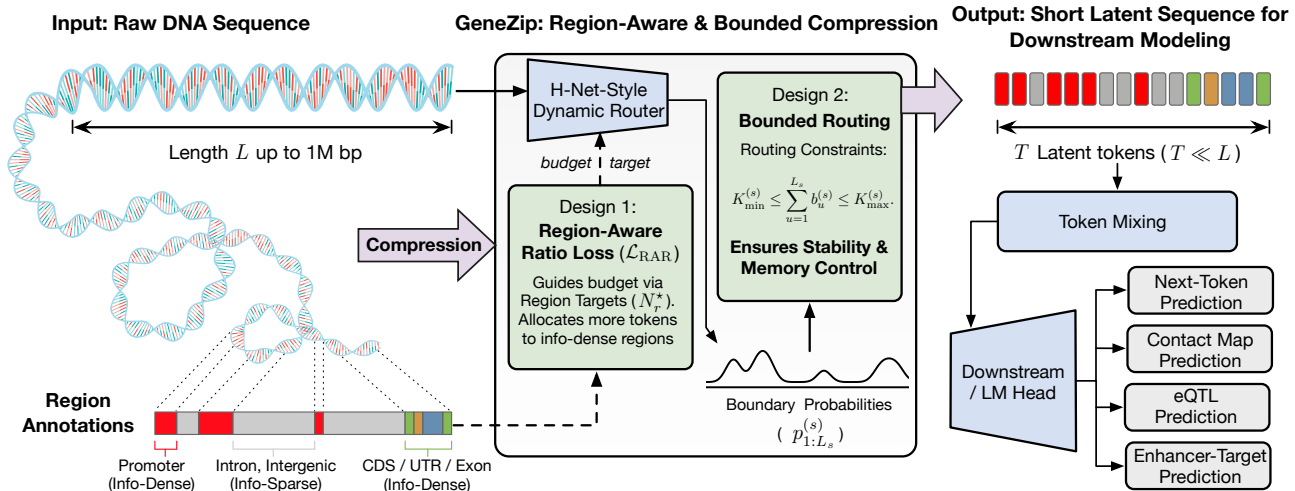


Figure 1. GeneZip overview. GeneZip compresses ultra-long DNA into a much shorter latent token sequence via hierarchical dynamic routing. During training, GeneZip uses Region-Aware Ratio (RAR) loss to learn a region-adaptive token compression budget, while bounded routing enforces global token-count constraints for stable training. The compressed tokens are then processed by an arbitrary token-mixing backbone for downstream long-range tasks. Notably, once trained, GeneZip can compress unseen raw DNA sequences *without* requiring annotations at inference time.

ing:

$$\begin{aligned}
 z_{1:T} &= \text{Encode}(x_{1:L}), & T \ll L, \\
 z'_{1:T} &= \text{TokenMixing}(z_{1:T}), \\
 \hat{y} &= \text{Decode}(z'_{1:T}).
 \end{aligned} \tag{1}$$

Here $\text{Encode}(\cdot)$ compresses raw DNA into a shorter latent sequence $z_{1:T}$, $\text{TokenMixing}(\cdot)$ models interactions among the T latent tokens, and $\text{Decode}(\cdot)$ maps mixed representations to pre-training or downstream task outputs.

In long-context DNA models, the dominant compute and memory typically sit in the token-mixing backbone (e.g., many Transformer layers (Vaswani et al., 2017) or long-sequence state-space mixers (Nguyen et al., 2023; Schiff et al., 2024)), while encoding/decoding are comparatively lightweight. This imbalance becomes acute as context grows: dense self-attention scales as $\mathcal{O}(T^2)$ per layer, making base-level token mixing ($T \approx L$) infeasible at megabase scale. A common strategy is therefore to downsample early so that deep layers operate on shorter sequences (e.g., U-Net style multi-scale processing in long-range sequence-to-function models (Avsec et al., 2021; 2026)).

However, most downsampling operators are uniform and static (fixed stride/pooling), implicitly allocating uniform resolution to all genomic positions. This is mismatched to genomic information density: for many tasks, a small subset of positions (e.g., promoters, splice junctions, UTR boundaries, coding regions, regulatory motifs) drive most of the signal, while large fractions of intronic and intergenic DNA are weakly informative. Uniform token allocation therefore wastes token budget on low-yield regions while undersampling high-yield regions.

Motivated by this, we propose **GeneZip**, a region-adaptive compression module that learns *non-uniform* token allocation over ultra-long DNA. As illustrated in Figure 1, GeneZip realizes the $\text{Encode}(\cdot)$ function with learned, content-dependent compression. Building on H-Net style hierarchical dynamic chunking and routing (Hwang et al., 2025), it learns variable-length segmentation and pooling end-to-end, producing compact token sequences that make expensive token mixing feasible at megabase scale. We inject a lightweight structural prior using only gene-structure annotations including, CDS, UTR, exon, intron, promoter, and intergenic regions. Specifically, we supervise region-wise token budgets with a Region-Aware Ratio (RAR) loss, encouraging higher resolution in information-dense regions and stronger compression elsewhere, *without* using functional assay labels (Hi-C, CAGE, ATAC/ChIP, GTEx, etc.) to train the compressor.

Throughout, we measure compression by base-pairs-per-token, denoted as $\text{BPT} := \frac{L}{T}$.

3.2. GeneZip encoder: hierarchical genomic compression with region-aware supervision

GeneZip instantiates $\text{Encode}(\cdot)$ with a multi-stage hierarchical genomic compression mechanism inspired by H-Net (Hwang et al., 2025). At each stage, the encoder (i) adaptively partitions a long sequence into variable-length chunks and (ii) pools each chunk into one token, so that deep token mixing can be applied on a much shorter sequence. Unlike fixed-stride pooling, the chunk boundaries are learned and depend on the input sequence.

Dynamic Routing module. GeneZip maintains continuous sequence representations at multiple resolutions. We start from base-level embeddings $h_{1:L_1}^{(1)} = \text{Embed}(x_{1:L})$ with $L_1 = L$. At routing stage $s \in \{1, \dots, S\}$, the stage- s encoder $E^{(s)}$ produces per-position representations $\hat{h}_{1:L_s}^{(s)} = E^{(s)}(h_{1:L_s}^{(s)})$, where L_s is the current sequence length at stage s . Following H-Net (Hwang et al., 2025), we induce adaptive boundaries by measuring the representation shift between adjacent positions in $\hat{h}^{(s)}$. We compute boundary probabilities $p_t^{(s)}$ via cosine *dissimilarity* between adjacent projected representations:

$$q_t^{(s)} = W_q^{(s)} \hat{h}_t^{(s)}, \quad k_t^{(s)} = W_k^{(s)} \hat{h}_t^{(s)}, \quad (2)$$

$$p_t^{(s)} = \begin{cases} 1, & t = 1, \\ \frac{1}{2} \left(1 - \frac{(q_t^{(s)})^\top k_{t-1}^{(s)}}{\|q_t^{(s)}\| \|k_{t-1}^{(s)}\|} \right), & t = 2, \dots, L_s, \end{cases} \quad (3)$$

$$p_t^{(s)} \in [0, 1], \quad \tilde{b}_t^{(s)} = \mathbb{1}\{p_t^{(s)} \geq 0.5\}. \quad (4)$$

By definition $p_1^{(s)} = 1$, ensuring each sequence begins with a boundary. Intuitively, when consecutive representations span a contextual shift, their cosine similarity decreases and the corresponding boundary probability $p_t^{(s)}$ increases.

Hierarchical dynamic chunking. At routing stage $s \in \{1, \dots, S\}$, the encoder operates on a sequence of length L_s and predicts boundary probabilities $\{p_t^{(s)}\}_{t=1}^{L_s}$ using the routing module above. We first threshold them into a provisional boundary mask $\{\tilde{b}_t^{(s)}\}_{t=1}^{L_s}$, and then apply bounded routing (Sec. 3.3) to obtain a length-controlled final mask $b^{(s)} = \Pi(\tilde{b}^{(s)}; p^{(s)})$. The final mask $\{b_t^{(s)}\}_{t=1}^{L_s}$ partitions the sequence into variable-length chunks. Each chunk is pooled into a single representation, producing a shorter sequence of length $L_{s+1} = \sum_{t=1}^{L_s} b_t^{(s)}$. The pooled sequence is then served as the input for the further stage, denoted as $h_{1:L_{s+1}}^{(s+1)}$.

After S stages, the encoder outputs $z_{1:T} = h_{1:L_{S+1}}^{(S+1)}$ with $T = L_{S+1}$. Compared to uniform striding, the learned boundary policy yields non-uniform resolution: segments with frequent boundaries receive more tokens.

Region supervision via gene structure. To make the compression biologically aligned and controllable, we supervise the *region-wise* token density using gene-structure annotations. Concretely, each base position t is assigned a genomic region label $r(t) \in \mathcal{R}$ (e.g. CDS, promoter, and intergenic regions). These region labels are used only to define supervision targets (RAR); the boundary predictor itself is trained to depend only on sequence, enabling annotation-free compression at inference.

We specify a global base target N (in BPT space) and a

region multiplier μ_r for each $r \in \mathcal{R}$, yielding a region target

$$N_r^* = N \cdot \mu_r. \quad (5)$$

Intuitively, smaller μ_r means *higher* resolution (more tokens) and larger μ_r means *stronger* compression. For example, one can set multipliers such as: promoter = 1, CDS = 1, UTR = 2, exon = 2, intron = 8, near-gene intergenic = 8, distal-intergenic = 16, to encourage GeneZip to learn to compress less on genic related regions and therefore allocates more compute on genic information.

Region-Aware Ratio (RAR) loss. RAR enforces region-specific compression by aligning region-wise keep rates across S routing stages. Given the region target N_r^* (Eq. 5), we geometrically factorize it over stages and define the per-stage target compression and keep rate:

$$N_r^{*(s)} \triangleq (N_r^*)^{1/S}, \quad \tau_r^{*(s)} \triangleq \frac{1}{N_r^{*(s)}}, \quad s = 1, \dots, S. \quad (6)$$

At stage s , each position $t \in \{1, \dots, L_s\}$ is associated with a region label $r^{(s)}(t) \in \mathcal{R}$ by propagating base-level annotations through the current segmentation (e.g., assigning each chunk the majority region label of the bases it covers). Let $L_r^{(s)} \triangleq \sum_{t=1}^{L_s} \mathbb{1}\{r^{(s)}(t) = r\}$. We define the empirical/expected keep rates:

$$F_r^{(s)} \triangleq \frac{1}{L_r^{(s)}} \sum_{t=1}^{L_s} \mathbb{1}\{r^{(s)}(t) = r\} b_t^{(s)}, \quad (7)$$

$$G_r^{(s)} \triangleq \frac{1}{L_r^{(s)}} \sum_{t=1}^{L_s} \mathbb{1}\{r^{(s)}(t) = r\} p_t^{(s)}.$$

We then apply the ratio loss with target compression $N_r^{*(s)}$:

$$\mathcal{L}_{\text{RAR}}^{(r,s)} = \frac{N_r^{*(s)}}{N_r^{*(s)} - 1} \left((N_r^{*(s)} - 1) F_r^{(s)} G_r^{(s)} + (1 - F_r^{(s)})(1 - G_r^{(s)}) \right). \quad (8)$$

Intuition. RAR loss couples the realized keep rate $F_r^{(s)}$ (after projection) and its expectation $G_r^{(s)}$ (before projection) to match the target $\tau_r^{*(s)}$. When $F_r^{(s)} = G_r^{(s)}$, Eq. (8) is minimized at $F_r^{(s)} = G_r^{(s)} = \tau_r^{*(s)}$ with $\mathcal{L}_{\text{RAR}}^{(r,s)} = 1$; if $F_r^{(s)}$ is too high/low, the gradient signal pushes $p_t^{(s)}$ down/up in region r , respectively. The overall RAR loss is the region-mass weighted sum across regions and stages:

$$\mathcal{L}_{\text{RAR}} = \sum_{s=1}^S \sum_{r \in \mathcal{R}} \pi_r^{(s)} \mathcal{L}_{\text{RAR}}^{(r,s)}, \quad \pi_r^{(s)} \triangleq \frac{L_r^{(s)}}{L_s}. \quad (9)$$

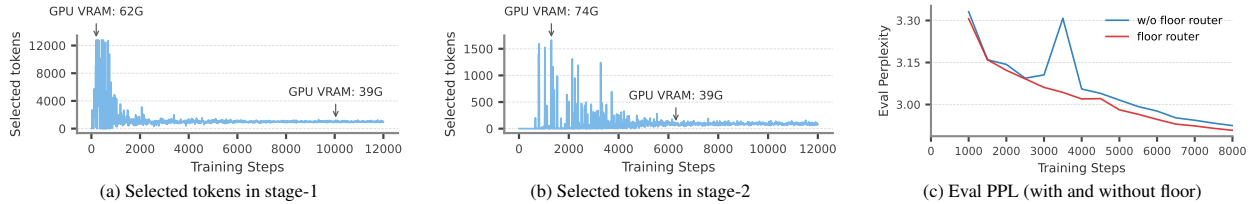


Figure 2. Why bounded routing is necessary. (a) In stage-1 compression, the router can be highly unstable early on and occasionally selects an excessively large number of tokens, which risks memory blow-up; a *ceiling* constraint prevents such pathological spikes. (b) In stage-2 compression, the router may collapse to selecting too few tokens (often near 1) at the beginning, which can induce training spikes and slow down optimization; a *floor* constraint enforces a minimum token budget for stable learning. (c) The floor constraint yields smoother and more favorable perplexity trajectories compared to training without it.

3.3. Bounded Routing for Stable Training

Under aggressive compression, as shown in Figure 2, unconstrained routing can be unstable early in training: it may either select too many boundaries (triggering GPU memory spikes) or collapse to too few (reducing effective capacity), both of which destabilize optimization. We stabilize training by enforcing a per-stage token-budget interval and projecting routing decisions onto this feasible set.

Reference token budget. At routing stage $s \in \{1, \dots, S\}$, the router predicts boundary probabilities $p_{1:L_s}^{(s)}$ and produces a provisional hard mask $\tilde{b}^{(s)}$ (e.g., by thresholding). We use a stage-wise keep-rate target $\tau^{(s)}$ as the reference budget, where $\prod_{s=1}^S \tau^{(s)} = 1/N$ and we use the uniform schedule $\tau^{(s)} = N^{-1/S}$ in this work. Given current length L_s , the reference token budget is $K^{(s)} \triangleq \tau^{(s)} L_s$. We define a floor and ceiling around $K^{(s)}$:

$$K_{\min}^{(s)} = \rho_{\min}^{(s)} K^{(s)}, \quad K_{\max}^{(s)} = \rho_{\max}^{(s)} K^{(s)}. \quad (10)$$

Projection (bounded routing). We compute a projected mask $b^{(s)} = \Pi(\tilde{b}^{(s)}; p^{(s)})$ that satisfies

$$K_{\min}^{(s)} \leq \sum_{t=1}^{L_s} b_t^{(s)} \leq K_{\max}^{(s)}. \quad (11)$$

The projection flips the smallest number of boundary decisions using $p^{(s)}$ as confidence scores: if $\sum_t \tilde{b}_t^{(s)} < K_{\min}^{(s)}$, we turn on boundaries at positions with the largest $p_t^{(s)}$ among those with $\tilde{b}_t^{(s)} = 0$; if $\sum_t \tilde{b}_t^{(s)} > K_{\max}^{(s)}$, we turn off boundaries at positions with the smallest $p_t^{(s)}$ among those with $\tilde{b}_t^{(s)} = 1$. The first position in each segment is always kept to prevent collapse.

3.4. Training and Inference

Training objective. Following H-Net (Hwang et al., 2025), we train GeneZip end-to-end with a language-modeling objective combined with the multi-stage RAR regularizer. Let \mathcal{L}_{NTP} denote base-level next-token cross-entropy. The overall objective is: $\mathcal{L} = \mathcal{L}_{\text{NTP}} + \alpha \mathcal{L}_{\text{RAR}}$, where α controls the strength of region-aware compression supervision.

Annotation-free inference. Although gene-structure annotations are used to define RAR supervision during training, GeneZip can compress unseen DNA *without* annotations at inference time: boundaries are predicted from sequence, bounded routing enforces the global token budget, and the resulting tokens can be fed into any token-mixing backbone (Transformer/Mamba) and decoded for downstream tasks.

Inference efficiency and long-context scaling. Figure 3 reports end-to-end inference latency as a function of input length up to 1M bp (benchmarking details in Appendix A.4). Across all tested contexts, GeneZip remains consistently fast, and the latency gap widens markedly as sequences enter the hundreds-of-kilobases to megabase regime. In contrast, baseline long-context models that operate closer to base-level resolution exhibit rapidly increasing runtime with length, leading to multi-second latency at the longest inputs. This behavior is expected: GeneZip reduces the *effective* token-mixing length via region-adaptive compression, so computation is dominated by mixing over a much shorter latent sequence rather than the raw base-pair sequence. Together with the strong downstream results, this scaling profile supports GeneZip as a practical tokenizer-level infrastructure for ultra-long DNA modeling, complementing the end-to-end training-time gains reported in Table 3.

4. Experiments

We perform extensive experiments to evaluate the performance of our proposed GeneZip model. We first describe the pretraining corpus construction, leakage-safe splits, and the two-stage length scaling schedule (§4.1). We then benchmark pretraining behavior in terms of perplexity, achieved compression budget (BPT), and scaling with context length and model size (§4.2). Next, we analyze the learned routing policy with qualitative case studies in §4.3 and provide additional compression diagnostics in Appendix C. Finally, we assess downstream utility on three DNALong-Bench tasks (Cheng et al., 2025): contact map prediction (§4.4), eQTL prediction (§4.5), and enhancer–target gene prediction (Appendix §D).

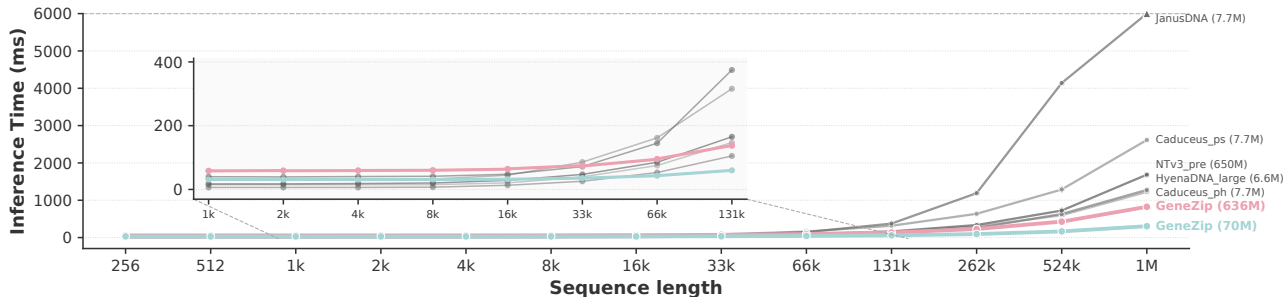


Figure 3. **Inference efficiency on ultra-long inputs.** End-to-end inference latency as a function of input sequence length (256 bp to 1M bp). GeneZip (70M/636M) remains consistently fast across the full range, while baseline long-context models exhibit sharply increasing latency as sequence length grows. The inset zooms into the short-to-mid regime (1K–131K) to highlight differences at smaller contexts.

4.1. Pretraining data and schedule

We construct our pretraining corpus from the human reference genome (GRCh38 primary assembly) using the GENCODE v49 *basic* gene annotation (Frankish et al., 2019). Each window is accompanied by a run-length encoded region segmentation over the 7-class taxonomy used throughout the paper (promoter, CDS, UTR, exon, intron, near-intergenic (NIG), and distal-intergenic (DIG)). To avoid data leakage, we do not use functional assay labels (Hi-C, CAGE, ATAC/ChIP, GTEX, etc.) to train our model. To tailor the corpus for DNALongBench evaluation and reduce benchmark leakage (Cheng et al., 2025; Rafi et al., 2025), we apply an explicit held-out filtering protocol when sampling *train/valid* windows. Specifically, we (i) exclude all DNALongBench validation and test intervals from the sampling pool, and (ii) hold out three entire chromosomes (chr8, chr9, chr10). Table 5 reports corpus statistics.

We perform two-stage pretraining for length scaling. First, we pre-train with 12.8K-bp contexts for a budget of 100B base pairs. Second, we continue pretraining with 128K-bp contexts for an additional 100B base pairs, keeping the same region taxonomy and training objective. Unless otherwise noted, we fix the base target N at 32 bp/token and use the same region-aware ratio target over seven regions (promoter:CDS:UTR:exon:intron:NIG:DIG = 1 : 1 : 2 : 2 : 8 : 8 : 16), encouraging higher effective resolution in gene-proximal and genic regions (defined in equation 5).

4.2. Pretraining evaluation (perplexity and budget control)

We first evaluate GeneZip’s language modeling performance and compare it with Mamba2 (Dao & Gu, 2024), UNet (Ronberger et al., 2015), and HNet (Hwang et al., 2025). For UNet, we implement an autoregressive UNet variant of our model by replacing the encoder with an autoregressive UNet. For HNet, we train two variants: a low-compression setting (HNet-3BPT, following the default configuration in (Hwang et al., 2025)) and a high-compression setting (HNet-128BPT). We train comparable-size baselines (70M-

84M) and GeneZip on 100B tokens of GENCODE data using a 12.8K context length. For GeneZip, we additionally study length scaling by continuing pretraining with a 128K context and also evaluate a 636M-parameter model. We report pretraining performance as per-region perplexity (PPL) on the validation set. For a detailed compression analysis, please refer to Appendix C.

Table 1 reports the overall evaluation PPL along with region-stratified PPL. We observe the following trends. First, Mamba2 and the low-compressed H-Net-3BPT serve as strong reference points, achieving the lowest PPLs under fixed or very fine-grained tokenizations. As expected, increasing the compression rate generally degrades performance; for example, H-Net-128BPT incurs a +0.38 PPL increase relative to the low-compression H-Net setting. Second, among encoder-based compression methods, GeneZip achieves the best overall PPL while operating at substantially higher effective compression. For instance, GeneZip-70M is the strongest highly compressed model, achieving the highest BPT = 137.6 while also attaining the lowest PPL across all regions. This suggests that GeneZip learns to identify region structure and allocate tokens more effectively. Finally, GeneZip exhibits favorable scaling with both context length and model size. Continuing pretraining to 128K context improves performance: GeneZip-70M-128K outperforms its 12.8K counterpart (GeneZip-70M) and incurs only a +0.24 PPL increase despite a more aggressive compression level (BPT = 169.2). The best results are obtained by GeneZip-636M-128K, indicating clear gains from combining longer-context pretraining with increased model capacity.

4.3. Case studies of GeneZip compression

To make the learned routing policy more concrete, we visualize the *boundary probability* (i.e., token-emission probability) along representative loci, together with a region taxonomy derived from GENCODE gene models (Frankish et al., 2019). Figure 4 overlays region labels (promoter/CDS/UTR/exon/intron/near-intergenic (NIG)) with per-base boundary probabilities produced by GeneZip-

Table 1. Region-wise autoregressive perplexity (PPL) on the validation dataset. We omit `dig` (distal-intergenic) because it is weakly constrained and often heavily compressed, making PPL less informative. **Bold** indicates the best (lowest) PPL among encoder-compression methods (U-Net, H-Net, GeneZip). Underline indicates the best PPL of small model trained at 12.8K length.

Model	BPT	Overall ↓	Prom. ↓	CDS ↓	UTR ↓	Exon ↓	Intron ↓	NIG ↓
<i>Backbone / fine-grained upper bounds</i>								
Mamba2-84M	1.0	2.4135	2.0494	2.4136	2.5608	2.6346	2.5076	2.4826
H-Net-3BPT-70M	3.0	2.4115	2.0694	2.4815	2.4306	2.8113	2.5462	2.4357
<i>Uniform / hierarchical compression baselines</i>								
U-Net-70M	128.0	2.8414	3.1335	3.4665	3.2389	3.0586	2.8415	2.6474
H-Net-128BPT-70M	122.2	2.7930	2.8940	3.4657	3.0241	3.0277	2.8270	2.6375
<i>GeneZip (region-aware compression)</i>								
GeneZip-70M	137.6	<u>2.7259</u>	<u>2.6765</u>	<u>3.4124</u>	2.9084	<u>2.9847</u>	<u>2.7761</u>	<u>2.6278</u>
GeneZip-70M-128K	169.2	2.6557	2.7520	3.0866	3.1236	3.0401	2.7350	2.5422
GeneZip-636M	137.0	2.6620	2.6094	2.8272	2.9311	3.2052	2.7724	2.5741
GeneZip-636M-128K	161.1	2.6484	2.8121	2.9647	3.1037	2.8712	2.6486	2.4941

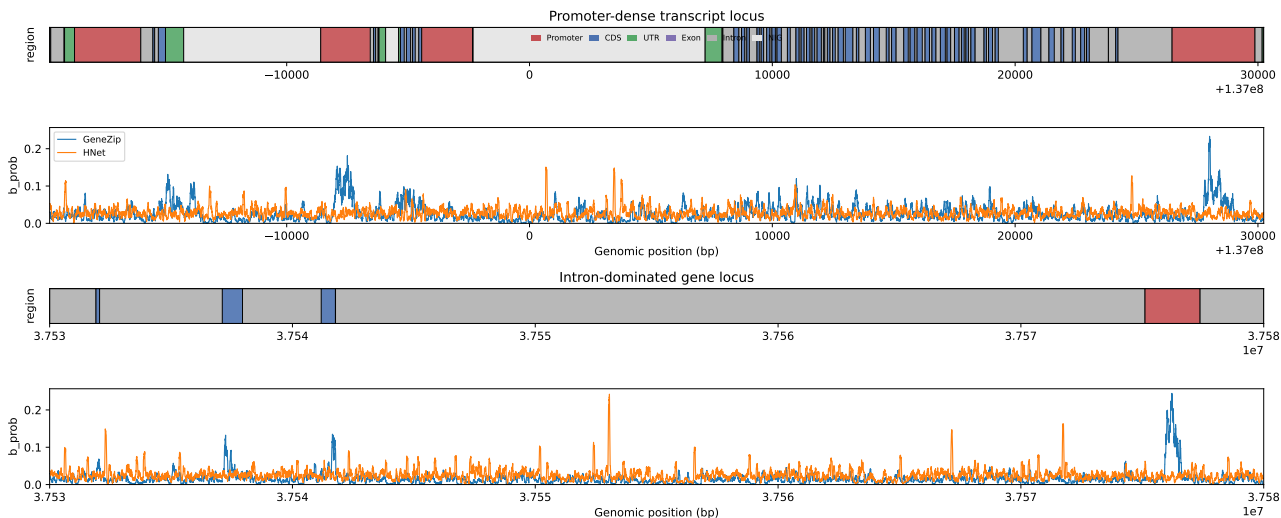


Figure 4. Case studies of region-adaptive compression. Region labels are induced from GENCODE gene models (Frankish et al., 2019) (promoter/CDS/UTR/exon/intron/near-intergenic (NIG)), and the curves plot per-base boundary probability for H-Net (Hwang et al., 2025) and GeneZip. We highlight two loci on chr9: a promoter-dense transcript locus (chr9:136,980,237–137,030,237; top) and an intron-dominated gene locus (chr9:37,530,000–37,580,000; bottom). Across both loci, GeneZip concentrates boundary mass in promoters and transcribed features, while suppressing diffuse boundaries in long intronic or intergenic spans.

70M (BPT = 137.6) and an H-Net-70M baseline (BPT = 122.2) (Hwang et al., 2025).

Across both loci, GeneZip exhibits region-adaptive allocation: boundary probability increases in promoters and transcribed features (exon/CDS/UTR) and decreases over long intronic and intergenic spans, yielding higher effective resolution where genomic signals are dense. In the promoter-dense locus (top), GeneZip maintains elevated boundary density around successive promoter segments and nearby transcribed landmarks, while compressing relatively feature-sparse intervals between them. In the intron-dominated locus (bottom), GeneZip suppresses diffuse boundaries across the long gene body and intergenic spans, while preserving sharp peaks near promoters and exon-related landmarks. Compared to H-Net, which produces a noisier boundary pro-

file with weaker alignment to region labels, GeneZip learns a more selective policy that better matches the Region-Aware Ratio objective.

4.4. Contact map prediction

We then assess how different downsampling modules affect representation learning on a long-range genomics benchmark, the contact map prediction (CMP) task in DNALongBench (Cheng et al., 2025). CMP is a two-dimensional regression task that maps a 1,048,576-bp DNA window to a binned chromatin contact map at 2,048-bp resolution. Following prior work (Zhou, 2022), we use a 2D CNN as the CMP predictor backbone, but vary its input features: mean-pooled bin embeddings produced by different sequence models. Specifically, we compare the following

Table 2. Contact map prediction on DNALongBench (Cheng et al., 2025). We report stratum-adjusted correlation coefficient (SCC) and Pearson correlation (Corr) across five cell lines, along with the average. Best results are in **bold**; second best are underlined.

Model	HFF		H1hESC		GM12878		IMR90		HCT116		Avg	
	SCC ↑	Corr ↑										
CNN-one-hot	0.0291	0.0571	0.0010	0.0297	0.0086	0.0321	0.0065	0.0302	0.0190	0.0203	0.0128	0.0339
Mamba2	0.1122	0.1631	0.1157	0.1657	0.0803	0.1134	0.1101	0.1588	0.1358	0.1532	0.1108	0.1508
HNet-3BPT	0.1263	0.1758	0.1235	0.1713	0.0966	0.1500	0.1178	0.1648	0.1586	0.1772	0.1245	0.1678
HNet-128BPT	0.1130	0.1626	0.1139	0.1597	0.0917	0.1405	0.1117	0.1597	0.1606	0.1811	0.1182	0.1607
UNet	0.1326	0.1853	<u>0.1306</u>	<u>0.1823</u>	<u>0.1043</u>	<u>0.1543</u>	0.1269	0.1782	<u>0.1625</u>	<u>0.1812</u>	<u>0.1314</u>	<u>0.1762</u>
GeneZip-AntiBioPrior	<u>0.1353</u>	<u>0.1878</u>	0.0652	0.1212	0.0554	0.1126	<u>0.1298</u>	<u>0.1821</u>	0.1583	0.1789	0.1088	0.1565
GeneZip	0.1399	0.1930	0.1386	0.1907	0.1073	0.1604	0.1310	0.1833	0.1634	0.1842	0.1360	0.1823

Table 3. DNA-LongBench eQTL tasks (AUROC; higher is better). The Best result in each dataset column is **bolded**, the second best is underlined. **Training time** reports the training time measured on the Artery Tibial task.

Model	Time (min)	eQTL Datasets (AUROC)								
		Artery	Adipose	Fibro	Muscle	Nerve	Skin (NSE)	Skin (SE)	Thyroid	Blood
Expert model(Cheng et al., 2025)	-	0.741	0.736	0.639	0.621	0.683	0.710	0.700	0.612	0.689
CNN(Cheng et al., 2025)	-	0.576	0.551	0.547	0.502	0.516	0.499	0.499	0.487	0.577
HyenaDNA(Cheng et al., 2025)	210	0.479	0.513	0.584	0.487	0.511	0.471	0.544	0.529	0.512
Caduceus-Ph(Cheng et al., 2025)	435	0.547	0.541	0.597	0.538	0.588	0.586	0.574	0.527	0.594
Caduceus-PS(Cheng et al., 2025)	891	0.536	0.519	0.549	0.523	0.552	0.529	0.541	0.547	0.542
HNet(Hwang et al., 2025)	65	0.781	0.676	0.785	0.880	0.862	<u>0.876</u>	0.862	0.745	0.715
JanusDNA(Dunn et al., 2025)	2520	<u>0.852</u>	<u>0.769</u>	<u>0.802</u>	0.864	0.914	0.903	0.846	0.793	0.821
Ntv3-100M-pre(Boshar et al., 2025)	117	0.805	0.744	0.698	0.798	0.885	0.886	0.727	0.778	0.808
GeneZip	50	0.860	0.781	0.806	0.881	<u>0.886</u>	0.861	0.868	0.795	0.821

representations: one-hot DNA embeddings (CNN-one-hot); Mamba2 without compression; UNet with uniform compression at 128 bp per token; HNet with two compression targets (HNet-3BPT and HNet-128BPT); GeneZip-AntiBioPrior, trained with an anti-biological region-aware ratio target (promoter:CDS:UTR:exon:intron:NIG:DIG = 32:16:8:4:2:4:1), which intentionally allocates coarser compression to genic regions; and GeneZip.

Table 2 summarizes CMP results. A key observation is that aggressively increasing the compression rate in adaptive routing can hurt downstream structure prediction: pushing HNet from 3BPT to 128BPT reduces the average SCC/Corr, indicating that high-ratio adaptive compression on genomic sequences is challenging and can readily discard task-relevant information for CMP. In contrast, GeneZip couples adaptive routing with a biologically grounded Region-Aware Ratio (RAR) objective and achieves the best performance on every cell line under both SCC and Corr, reaching a best average of 0.1360/0.1823, outperforming uniform compression (UNet), and learnable compression (HNet) baselines. Additionally, the GeneZip-AntiBioPrior negative control causes significant performance downgrade on H1hESC and GM12878 (0.0652/0.1212 and 0.0554/0.1126) compared with GeneZip. Together, these results support that the RAR objective steers the compressor toward a transferable biological prior, yielding representations that better preserve regulatory and genic cues needed for 3D genome structure prediction.

4.5. eQTL prediction

We evaluate long-range variant effect modeling on the nine DNALongBench (Cheng et al., 2025) eQTL classification tasks. Table 3 reports AUROC across tissues, along with end-to-end fine-tuning time under an identical pipeline (training time measured on the Artery Tibial task). More experimental settings can be found at Appendix A.3.

In terms of efficiency, models with explicit downsampling/compression modules (NTv3 (Boshar et al., 2025), HNet, and GeneZip) fine-tune substantially faster than those without (HyenaDNA and Caduceus), underscoring the need to reduce effective sequence length before token mixing in long-context genomic tasks. GeneZip is the fastest overall, completing training in 50 minutes, compared to 210 minutes for HyenaDNA and 435/891 minutes for Caduceus variants.

In terms of effectiveness, GeneZip outperforms HNet on 8 of 9 tissues, suggesting that region-aware pretraining provides a transferable inductive bias beyond learning an adaptive compressor. Overall, GeneZip matches the strongest baseline, JanusDNA: it achieves the best AUROC on 6/9 tissues (Artery, Adipose, Fibro, Muscle, Skin (SE), and Thyroid) and ties for the best score on Blood (0.821), while enjoying a 50.4× speedup (50 vs. 2520 minutes).

5. Conclusion

We propose GeneZip, a region-aware DNA compressor that uses bounded dynamic routing and a region-aware compression objective to reallocate token budget to emphasize information-dense regions. GeneZip achieves 137.6× compression with only a 0.31 perplexity increase, matches or surpasses existing SoTA JanusDNA on various long-range tasks, and enables much larger models at megabase context (e.g., 636M parameters at 1M bp, 82.6× larger than JanusDNA). Overall, GeneZip demonstrates that learned compression can jointly scale context and capacity on a single A100 80GB GPU, making genome-scale modeling substantially more practical.

References

- Avsec, Z., Agarwal, V., Visentin, D., Ledsam, J. R., Grabska-Barwinska, A., Taylor, K. R., Assael, Y., Jumper, J., Kohli, P., and Kelley, D. R. Effective gene expression prediction from sequence by integrating long-range interactions. *Nature Methods*, 18(10):1196–1203, 2021. doi: 10.1038/s41592-021-01252-x.
- Avsec, Z., Latysheva, N., Cheng, J., Novati, G., Taylor, K. R., Ward, T., Bycroft, C., Nicolaisen, L., Arvaniti, E., Pan, J., Thomas, R., Dutordoir, V., Perino, M., De, S., Karollus, A., Gayoso, A., Sargeant, T., Mottram, A., Wong, L. H., Drotar, P., Kosiorek, A., Senior, A., Tanburn, R., Applebaum, T., Basu, S., Hassabis, D., and Kohli, P. Advancing regulatory variant effect prediction with alphagenome. *Nature*, 649(8099):1206–1218, January 2026. doi: 10.1038/s41586-025-10014-0.
- Boshar, S., Evans, B., Tang, Z., Picard, A., Adel, Y., Lorbeer, F. K., Rajesh, C., Karch, T., Sidbon, S., Emms, D., Mendoza-Revilla, J., Al-Ani, F., Seitz, E., Schiff, Y., Bornachot, Y., Hernandez, A., Lopez, M., Laterre, A., Beguir, K., Koo, P., Kuleshov, V., Stark, A., de Almeida, B. P., and Pierrot, T. A foundational model for joint sequence-function multi-species modeling at scale for long-range genomic prediction. bioRxiv, December 2025. URL <https://www.biorxiv.org/content/10.64898/2025.12.22.695963v1>. bioRxiv preprint.
- Brix, G., Durrant, M. G., Ku, J., Poli, M., Brockman, G., Chang, D., Gonzalez, G. A., King, S. H., Li, D. B., Merchant, A. T., Naghipourfar, M., Nguyen, E., Ricci-Tam, C., Romero, D. W., Sun, G., Taghibakshi, A., Vorontsov, A., Yang, B., Deng, M., Gorton, L., Nguyen, N., Wang, N. K., Adams, E., Baccus, S. A., Dillmann, S., Ermon, S., Guo, D., Ilango, R., Janik, K., Lu, A. X., Mehta, R., Mofrad, M. R., Ng, M. Y., Pannu, J., Re, C., Schmok, J. C., St. John, J., Sullivan, J., Zhu, K., Zynda, G., Balsam, D., Collison, P., Costa, A. B., Hernandez-Boussard, T., Ho, E., Liu, M.-Y., McGrath, T., Powell, K., Burke, D. P., Goodarzi, H., Hsu, P. D., and Hie, B. Genome modeling and design across all domains of life with evo 2. *bioRxiv*, 2025. doi: 10.1101/2025.02.18.638918. URL <https://www.biorxiv.org/content/early/2025/02/21/2025.02.18.638918>.
- Brown, T. B., Mann, B., Ryder, N., Subbiah, M., Kaplan, J. D., Dhariwal, P., Neelakantan, A., Shyam, P., Sastry, G., Askell, A., et al. Language models are few-shot learners. In *Advances in Neural Information Processing Systems*, volume 33, 2020. URL <https://arxiv.org/abs/2005.14165>.
- Cheng, W., Song, Z., Zhang, Y., Wang, S., Wang, D., Yang, M., Li, L., and Ma, J. DNALongBench: a benchmark suite for long-range DNA prediction tasks. *Nature Communications*, 16(1):10108, 2025. doi: 10.1038/s41467-025-65077-4.
- Dalla-Torre, H., Gonzalez, L., Mendoza-Revilla, J., Lopez Carranza, N., Grzywaczewski, A. H., Oteri, F., Dallago, C., Trop, E., de Almeida, B. P., Sirelkhatim, H., Richard, G., Skwark, M., Beguir, K., Lopez, M., and Pierrot, T. Nucleotide transformer: building and evaluating robust foundation models for human genomics. *Nature Methods*, 22(2):287–297, 2025. doi: 10.1038/s41592-024-02523-z.
- Dao, T. and Gu, A. Transformers are SSMs: Generalized models and efficient algorithms through structured state space duality. In Salakhutdinov, R., Kolter, Z., Heller, K., Weller, A., Oliver, N., Scarlett, J., and Berkenkamp, F. (eds.), *Proceedings of the 41st International Conference on Machine Learning*, volume 235 of *Proceedings of Machine Learning Research*, pp. 10041–10071. PMLR, July 2024. URL <https://proceedings.mlr.press/v235/dao24a.html>.
- Duan, Q., Huang, B., Song, Z., Lehmann, I., Gu, L., Eils, R., and Wild, B. Janusdna: A powerful bi-directional hybrid DNA foundation model, May 2025. NeurIPS 2025.
- ENCODE Project Consortium. An integrated encyclopedia of DNA elements in the human genome. *Nature*, 489(7414):57–74, 2012. doi: 10.1038/nature11247. URL <https://www.nature.com/articles/nature11247>.
- Frankish, A., Diekhans, M., Ferreira, A.-M., Johnson, R., Jungreis, I., Loveland, J., Mudge, J. M., Sisu, C., Wright, J., Armstrong, J., Barnes, I. F., Berry, A., Bignell, A., Carbonell Sala, S., Chrast, J., Cunningham, F., Di Domenico, T., Donaldson, S., Fiddes, I. T., García Girón, C., Gonzalez, J. M., Grego, T., Hardy, M., Hourlier, T., Hunt, T., Izuogu, O. G., Lagarde, J., Martin, F. J., Martínez, L., Mohanan, S., Muir, P., Navarro, F. C. P., Parker, A., Pei, B., Pozo, F., Ruffier, M., Schmitt, B. M., Stapleton, E., Suner, M.-M., Sycheva, I., Uszczyńska-Ratajczak, B., Xu, J., Yates, A., Zerbino, D., Zhang, Y., Aken, B., Choudhary, J. S., Gerstein, M., Guigó, R., Hubbard, T. J. P., Kellis, M., Paten, B., Reymond, A., Tress, M. L., and Flicek, P. GENCODE reference annotation for the human and mouse genomes. *Nucleic Acids Research*, 47(D1):D766–D773, 2019. doi: 10.1093/nar/gky955.
- Fudenberg, G., Kelley, D. R., and Pollard, K. S. Predicting 3D genome folding from DNA sequence with akita. *Nature Methods*, 17(11):1111–1117, 2020. doi: 10.1038/s41592-020-0958-x.
- Grattafiori, A., Dubey, A., Jauhri, A., Pandey, A., Kadian, A., Al-Dahle, A., Letman, A., Mathur, A., Schelten, A.,

- Vaughan, A., et al. The llama 3 herd of models, July 2024.
- Hwang, S., Wang, B., and Gu, A. Dynamic chunking for end-to-end hierarchical sequence modeling, July 2025. H-Net.
- International Human Genome Sequencing Consortium. Initial sequencing and analysis of the human genome. *Nature*, 409(6822):860–921, 2001. doi: 10.1038/35057062. URL <https://www.nature.com/articles/35057062>.
- Ji, Y., Zhou, Z., Liu, H., and Davuluri, R. V. DNABERT: pre-trained bidirectional encoder representations from transformers model for dna-language in genome. *Bioinformatics*, 37(15):2112–2120, 2021. doi: 10.1093/bioinformatics/btab083.
- Kallini, J., Murty, S., Manning, C. D., Potts, C., and Csordás, R. Mrt5: Dynamic token merging for efficient byte-level language models. In *International Conference on Learning Representations*, 2025. URL <https://arxiv.org/abs/2410.20771>.
- Kudo, T. and Richardson, J. Sentencepiece: A simple and language independent subword tokenizer and detokenizer for neural text processing, August 2018.
- Ledneva, D. and Kuznetsov, D. Ldarnet: Dna adaptive representation network with learnable tokenization for genomic modeling. OpenReview, ICLR 2026 Conference Submission, September 2025. Under review.
- Li, S., Wang, Z., Liu, Z., Wu, D., Tan, C., Zheng, J., Huang, Y., and Li, S. Z. VQDNA: Unleashing the power of vector quantization for multi-species genomic sequence modeling. In Salakhutdinov, R., Kolter, Z., Heller, K., Weller, A., Oliver, N., Scarlett, J., and Berkenkamp, F. (eds.), *Proceedings of the 41st International Conference on Machine Learning*, volume 235 of *Proceedings of Machine Learning Research*, pp. 28717–28733. PMLR, July 2024. URL <https://proceedings.mlr.press/v235/li24bm.html>.
- Lindblad-Toh, K., Garber, M., Zuk, O., Lin, M. F., Parker, B. J., Washietl, S., Kheradpour, P., Ernst, J., Jordan, G., Mauceli, E., Ward, L. D., Lowe, C. B., Holloway, A. K., Clamp, M., Gnerre, S., Alföldi, J., Beal, K., Chang, J., Clawson, H., Cuff, J., Di Palma, F., Fitzgerald, S., Flicek, P., Guttman, M., Hubisz, M. J., Jaffe, D. B., Jungreis, I., Kent, W. J., Kostka, D., Lara, M., Martins, A. L., Masingham, T., Moltke, I., Raney, B. J., Rasmussen, M. D., Robinson, J., Stark, A., Vilella, A. J., Wen, J., Xie, X., Zody, M. C., Broad Institute Sequencing Platform and Whole Genome Assembly Team, Baldwin, J., Bloom, T., Chin, C. W., Heiman, D., Nicol, R., Nusbaum, C., Young, S., Wilkinson, J., Worley, K. C., Kovar, C. L., Muzny, D. M., Gibbs, R. A., Baylor College of Medicine Human Genome Sequencing Center Sequencing Team, Cree, A., Dihm, H. H., Fowler, G., Jhangiani, S., Joshi, V., Lee, S., Lewis, L. R., Nazareth, L. V., Okwuonu, G., Santibanez, J., Warren, W. C., Mardis, E. R., Weinstock, G. M., Wilson, R. K., Genome Institute at Washington University, Delehaunty, K., Dooling, D., Fronik, C., Fulton, L., Fulton, B., Graves, T., Minx, P., Sodergren, E., Birney, E., Margulies, E. H., Herrero, J., Green, E. D., Haussler, D., Siepel, A., Goldman, N., Pollard, K. S., Pedersen, J. S., Lander, E. S., and Kellis, M. A high-resolution map of human evolutionary constraint using 29 mammals. *Nature*, 478(7370):476–482, 2011. doi: 10.1038/nature10530.
- Nguyen, E., Poli, M., Faizi, M., Thomas, A., Birch-Sykes, C., Wornow, M., Patel, A., Rabideau, C., Massaroli, S., Bengio, Y., Ermon, S., Baccus, S. A., and Ré, C. Hye-naDNA: Long-range genomic sequence modeling at single nucleotide resolution, June 2023. NeurIPS 2023 Spotlight.
- Nguyen, E., Poli, M., Durrant, M. G., Kang, B., Katrekar, D., Li, D. B., Bartie, L. J., Thomas, A. W., King, S. H., Brix, G., Sullivan, J., Ng, M. Y., Lewis, A., Lou, A., Ermon, S., Baccus, S. A., Hernandez-Boussard, T., Re, C., Hsu, P. D., and Hie, B. L. Sequence modeling and design from molecular to genome scale with evo. *Science*, 386(6723):ead09336, 2024. doi: 10.1126/science.ado9336. URL <https://pubmed.ncbi.nlm.nih.gov/39541441/>.
- Pagnoni, A., Pasunuru, R., Rodriguez, P., Nguyen, J., Muller, B., Li, M., Zhou, C., Yu, L., Weston, J., Zettlemoyer, L., et al. Byte latent transformer: Patches scale better than tokens, December 2024.
- Qiao, L., Ye, P., Ren, Y., Bai, W., Liang, C., Ma, X., Dong, N., and Ouyang, W. Model decides how to tokenize: Adaptive DNA sequence tokenization with mxdna, December 2024. NeurIPS 2024.
- Radford, A., Wu, J., Child, R., Luan, D., Amodei, D., and Sutskever, I. Language models are unsupervised multitask learners. OpenAI Technical Report, 2019. URL https://cdn.openai.com/better-language-models/language_models_are_unsupervised_multitask_learners.pdf.
- Rafi, A. M., Kiyota, B., Yachie, N., and de Boer, C. G. Detecting and avoiding homology-based data leakage in genomic machine learning. *bioRxiv*, January 2025. doi: 10.1101/2025.01.22.634321. URL <https://www.biorxiv.org/content/10.1101/2025.01.22.634321v1>. Preprint.

- Ronneberger, O., Fischer, P., and Brox, T. U-Net: Convolutional networks for biomedical image segmentation. In *Medical Image Computing and Computer-Assisted Intervention (MICCAI)*, pp. 234–241, 2015. doi: 10.1007/978-3-319-24574-4_28. URL https://link.springer.com/chapter/10.1007/978-3-319-24574-4_28.
- Schiff, Y., Kao, C.-H., Gokaslan, A., Dao, T., Gu, A., and Kuleshov, V. Caduceus: Bi-directional equivariant long-range DNA sequence modeling. In *Proceedings of the 41st International Conference on Machine Learning*, volume 235 of *Proceedings of Machine Learning Research*, pp. 43632–43648. PMLR, 2024.
- Sennrich, R., Haddow, B., and Birch, A. Neural machine translation of rare words with subword units, August 2015.
- Slagle, K. Spacebyte: Towards deleting tokenization from large language modeling. In *Advances in Neural Information Processing Systems*, volume 37, 2024. URL <https://arxiv.org/abs/2404.14408>. NeurIPS 2024.
- Touvron, H., Martin, L., Stone, K., Albert, P., Almahairi, A., Babaei, Y., Bashlykov, N., Batra, S., Bhargava, P., Bhosale, S., et al. Llama 2: Open foundation and fine-tuned chat models, July 2023.
- Vaswani, A., Shazeer, N., Parmar, N., Uszkoreit, J., Jones, L., Gomez, A. N., Kaiser, L., and Polosukhin, I. Attention is all you need. In *Advances in Neural Information Processing Systems*, 2017.
- Xue, L., Barua, A., Constant, N., Al-Rfou, R., Narang, S., Kale, M., Roberts, A., and Raffel, C. Byt5: Towards a token-free future with pre-trained byte-to-byte models. *Transactions of the Association for Computational Linguistics*, 10:291–306, 2022. doi: 10.1162/tacl.a.00461. URL <https://aclanthology.org/2022.tacl-1.17/>.
- Yu, L., Simig, D., Flaherty, C., Aghajanyan, A., Zettlemoyer, L., and Lewis, M. Megabyte: Predicting million-byte sequences with multiscale transformers. In *Advances in Neural Information Processing Systems*, volume 36, pp. 78808–78823, 2023. URL <https://arxiv.org/abs/2305.07185>.
- Zhou, J. Sequence-based modeling of three-dimensional genome architecture from kilobase to chromosome scale. *Nature Genetics*, 54(5):725–734, 2022. doi: 10.1038/s41588-022-01065-4.
- Zhou, Z., Ji, Y., Li, W., Dutta, P., Davuluri, R. V., and Liu, H. DNABERT-2: Efficient foundation model and benchmark for multi-species genomes. In *International Conference on Learning Representations*, 2024.

A. Implementation Details

A.1. Pretraining Settings

We use a two-stage hierarchical dynamic chunking encoder with $S = 2$, where each stage is implemented with two Mamba2 layers. The token-mixing backbone consists of 15 Mamba2 layers. We pretrain GeneZip with region-aware compression using a fixed region taxonomy (*promoter*, *CDS*, *UTR*, *exon*, *intron*, *NIG*, *DIG*). Across both stages, we fix the global base budget to $N = 32$ bp/token and use the same region-aware ratio targets over the seven regions (*promoter*:*CDS*:*UTR*:*exon*:*intron*:*NIG*:*DIG* = 1 : 1 : 2 : 2 : 8 : 8 : 16). For bounded routing, we apply a shared absolute floor across all GeneZip models with $K_{\min}^{(s)} = 8$ for all stages s , meaning at least the top-8 tokens are kept in each routing layer. For the upper bound, the 70M model fits comfortably on an 80GB A100 and does not require a maximum constraint. In contrast, for the 636M model an upper bound is necessary, as routing can otherwise trigger CUDA out-of-memory (OOM) errors. We therefore set $K_{\max}^{(1)} = 30,000$ and $K_{\max}^{(2)} = 10,000$ to prevent OOM. Unless otherwise noted, all stages of GeneZip models and baseline models are trained on a total budget of 100B base pairs each.

Stage 1 (12.8K) pretraining. We train on `gencode_human_12.8k` with a maximum sequence length of 12,800 bp. We optimize with AdamW using learning rate 1×10^{-3} , weight decay 0.1, $(\beta_1, \beta_2) = (0.9, 0.95)$, a linear learning-rate schedule with 500 warmup steps, and gradient clipping to $\|g\|_2 \leq 2.0$. We fix effective batch size as 256 and train for 100B tokens using BF16 mixed precision. We evaluate using 3,000 validation samples.

Stage 2 (128K) pretraining. We continue training on `gencode_human_128k` with a maximum sequence length of 128,000 bp, initializing from the 12.8K checkpoint introduced above. We keep the same optimizer and schedule (AdamW; LR 1×10^{-3} ; 500 warmup steps; weight decay 0.1; $(\beta_1, \beta_2) = (0.9, 0.95)$; gradient clipping 2.0; BF16). We fix effective batch size as 256 and train for another 100B tokens using BF16 mixed precision. We evaluate using 3,000 validation samples.

A.2. Contact Map Prediction Experimental Settings

We evaluate DNALongBench’s contact map prediction (CMP) task by training a lightweight CNN contact-map head (Zhou, 2022) on top of frozen sequence representations, for each cell-type subset (HFF, H1hESC, GM12878, IMR90, HCT116). Specifically, we use a small convolutional head (projection dim 128; distance embedding dim 16; 2-layer 1D CNN kernel 5 with dropout 0.1; 3-layer 2D CNN with channels [64, 64, 64], kernel 3, dropout 0.1; symmetrized outputs). We optimize with AdamW using

Table 4. Pre-training hyperparameters for the GeneZip models.

	12.8K pre-train	128K pre-train
Dataset	gencode_human_12.8k	gencode_human_128k
Region loss weight α	0.03	0.03
Max length (bp)	12,800	128,000
Per-device batch size	32	4
Grad. accumulation	8	8
Update steps	30,600	24,414
Optimizer	AdamW	AdamW
Learning rate	1×10^{-3}	1×10^{-3}
LR schedule	Linear + warmup	Linear + warmup
Warmup steps	500	500
Weight decay	0.1	0.1
Adam (β_1, β_2)	(0.9, 0.95)	(0.9, 0.95)
Grad clip	2.0	2.0
Precision	BF16	BF16
Validation samples	3,000	3,000

learning rate 2×10^{-4} , weight decay 0, batch size 32, BF16 mixed precision, and gradient clipping $\|g\|_2 \leq 1.0$. We train for 5,000 update steps.

A.3. Expression Quantitative Trait Loci Prediction Experimental Settings

We evaluate the eQTL prediction task from DNA-LONGBENCH (Cheng et al., 2025) by fine-tuning a pretrained model with region-aware compression under a fixed 7-region taxonomy and ratio targets (promoter:CDS:UTR:exon:intron:NIG:DIG = 1 : 16 : 2 : 4 : 2 : 2 : 4). This task-specific allocation reflects a regulatory prior: we preserve higher resolution in promoter-proximal and gene-adjacent noncoding regions (promoter/intron/NIG) while allowing stronger compression in coding sequence (CDS) that is less informative for expression-modulating variants.

To stabilize supervised adaptation on limited labeled data and to isolate the effect of the learned compressor, we freeze the encoder (including the router and embedding layer) and optimize only the task head. We use AdamW with learning rate 2×10^{-4} , weight decay 0.1, $(\beta_1, \beta_2) = (0.9, 0.95)$, a linear learning-rate schedule with warmup ratio 0.1, and gradient clipping $\|g\|_2 \leq 1.0$ for long-context stability. Due to the long input length, we train for 3 epochs with per-device batch size 1 and gradient accumulation 8 (effective batch size 8 per device), using BF16 mixed precision.

A.4. Inference Latency Benchmark (Figure 3)

Figure 3 reports the inference-time scaling of each model as a function of input length. We measure the forward-pass latency on a single NVIDIA A100 80GB GPU with BF16 inference and batch size 1. For each context length $L \in \{256, 512, \dots, 1,048,576\}$ bp, we construct a length- L DNA string by repeating a fixed sequence snippet and

encode it into single-nucleotide token IDs.

Timing protocol. We time only the model forward pass, excluding model loading and input construction. For each (model, L) pair, we run 2 warm-up forward passes, followed by 10 timed runs. Each timed run synchronizes the device before and after the forward pass and uses to record wall-clock time. We report the mean of the per-forward latency in milliseconds in Figure 3.

B. Training Data Details

B.1. GENCODE-based pretraining corpus construction

We construct the human pretraining corpora from the GRCh38 primary assembly together with the GENCODE v49 *basic* gene annotation (Frankish et al., 2019).

Region taxonomy and priority overlay. We build a genome-wide region map and label each base with exactly one region under a deterministic priority order: promoter > cds > utr > exon > intron > nig > dig. Promoters are defined as symmetric windows around the transcript TSS (TSS ± 1 kbp). We further partition intergenic sequence into near-intergenic (NIG) and distal-intergenic (DIG) based on proximity to annotated transcription start sites (TSSs). After applying the region-priority overlay (so that promoter/genic regions take precedence), an intergenic base is labeled as NIG if it lies within 450 kbp (genomic distance) of any annotated TSS; otherwise it is labeled as DIG.

Sampling, splits, and formats. We create two corpora with fixed context lengths: 12.8K bp and 128K bp. For train/valid, windows are sampled with a mixture of center choices that increases coverage near transcription start sites and coding regions, alongside uniform sampling

Table 5. Statistics of the GENCODE-derived pretraining corpora used in this work. **Total BP** is reported in Mbp. Region columns report Mbp with within-split percentages in parentheses under our 7-region taxonomy: promoter, coding sequence (CDS), UTR, exon, intron, near-intergenic (NIG), and distal-intergenic (DIG). **N BP** reports ambiguous bases (N) in Mbp. The `test` split corresponds to contiguous, non-sampled windows from held-out chromosomes (`chr8`, `chr9`, `chr10`), while `train/valid` are sampled windows.

Dataset	Split	Total BP (M)	N BP (M)	Promoter	CDS	UTR	Exon	Intron	NIG	DIG
GENCODE-Human-12.8k	train	12160.00	0.16	1815.54 (14.93%)	324.84 (2.67%)	296.16 (2.44%)	190.66 (1.57%)	6758.93 (55.58%)	2636.61 (21.68%)	137.26 (1.13%)
	valid	640.00	0.01	96.56 (15.09%)	17.08 (2.67%)	15.51 (2.42%)	9.89 (1.55%)	355.94 (55.61%)	138.24 (21.60%)	6.79 (1.06%)
GENCODE-Human-128k	train	12672.00	0.63	1047.20 (8.26%)	223.82 (1.77%)	259.47 (2.05%)	174.46 (1.38%)	7546.70 (59.55%)	3266.07 (25.77%)	154.28 (1.22%)
	valid	128.00	0.01	10.52 (8.22%)	2.23 (1.74%)	2.72 (2.12%)	1.79 (1.40%)	77.64 (60.65%)	32.21 (25.17%)	0.90 (0.70%)
Held-out (<code>chr8</code> , <code>9</code> , <code>chr10</code>)		417.34	17.52	22.44 (5.38%)	3.42 (0.82%)	4.81 (1.15%)	5.11 (1.22%)	243.77 (58.41%)	117.50 (28.15%)	20.31 (4.87%)

across the remaining genome. Each window stores the raw DNA sequence together with a run-length encoded segmentation over the 7-region taxonomy. The `valid` split is an in-distribution holdout constructed with the same sampling procedure as `train`.

DNALongBench leakage filtering and held-out chromosomes. To tailor the corpus for DNALongBench evaluation and mitigate benchmark leakage (Cheng et al., 2025; Rafi et al., 2025), we remove all genomic intervals used by DNALongBench validation/test sets from the sampling pool for `train/valid`. In addition, we fully hold out the DNALongBench transcription-initiation held-out chromosomes `chr8`, `chr9`, and `chr10` during sampling. These chromosomes are reserved to construct a chromosome-level test split by tiling `chr8`, `chr9`, and `chr10` into contiguous, non-overlapping windows of the target context length (without sampling).

C. A Detailed Analysis of GeneZip’s Compression Performance

Evaluation protocol. We evaluate encoder-only checkpoints on the held-out chromosomes `chr8`, `chr9`, and `chr10` using contiguous 128 Kbp windows (3,262 windows in total). For each window, the encoder predicts a hard boundary mask (with reverse-complement averaging), inducing a variable-length tokenization; all metrics below are computed per window and then reported as mean \pm standard deviation.

Metrics. Let a window contain L bases $x_{1:L}$ and let boundary positions $0 = s_1 < s_2 < \dots < s_T < s_{T+1} = L$ define token spans $[s_t, s_{t+1})$. The *observed* base-per-token (BPT) is

$$\text{BPT}_{\text{obs}} := \frac{1}{T} \sum_{t=1}^T (s_{t+1} - s_t) = \frac{L}{T}. \quad (12)$$

Given region labels, let B_r be the number of bases assigned to region r in the window, and let N_r^* denote the *target* BPT for region r (Eq. 5). The *expected* BPT under the target

allocation is

$$\text{BPT}_{\text{exp}} := \frac{\sum_r B_r}{\sum_r B_r / N_r^*}, \quad (13)$$

and we report a global budget-matching ratio

$$\text{BPT-ratio} := \frac{\text{BPT}_{\text{obs}}}{\text{BPT}_{\text{exp}}}. \quad (14)$$

Note that BPT_{exp} is a base-count weighted harmonic mean of $\{N_r^*\}$, and $\text{BPT-ratio} = (\sum_r B_r / N_r^*) / T$ equals the ratio of expected-to-observed token counts.

To measure region-level budget adherence, we fractionally attribute each token to regions. Let \mathcal{R}_r be the set of base indices labeled as region r , and define the (fractional) token count assigned to region r as

$$T_r := \sum_{t=1}^T \frac{|[s_t, s_{t+1}) \cap \mathcal{R}_r|}{s_{t+1} - s_t}, \quad \hat{N}_r := \frac{B_r}{T_r}. \quad (15)$$

We then define the micro-averaged alignment error

$$\text{MicroErr} := \frac{1}{\sum_r B_r} \sum_r B_r \left| \log \frac{\hat{N}_r}{N_r^*} \right|. \quad (16)$$

MicroErr is an absolute log error: $\exp(\text{MicroErr})$ can be interpreted as the geometric mean multiplicative mismatch.

To characterize *where* token budget is spent, we report group-level enrichment over promoter, genetic (CDS/UTR/exon), and intergenic (intron/NIG/DIG) regions:

$$\text{Enrich}(g) := \frac{T_g / \sum_r T_r}{B_g / \sum_r B_r}, \quad (17)$$

$$T_g := \sum_{r \in g} T_r, \quad B_g := \sum_{r \in g} B_r.$$

Here, $\text{Enrich}(g) > 1$ indicates that the token budget is concentrated on group g relative to its genomic coverage. Finally, we report base-level perplexity

$$\text{PPL} := \exp \left(\frac{1}{L} \sum_{i=1}^L -\log p(x_i | x_{<i}) \right). \quad (18)$$

Lower perplexity indicates better language modeling quality.

Table 6. Pretraining evaluation of encoder-only checkpoints on held-out dataset. Best values are **bold**.

Model	Observed BPT (bp/token)	BPT-ratio ($\rightarrow 1$)	PPL \downarrow	MicroErr \downarrow	Intergenic enrich \downarrow	Promoter enrich \uparrow	Genic enrich \uparrow
H-Net-BPT128	1664.9 \pm 7943.4	11.50 \pm 54.27	2.8649	-	1.000 \pm 0.017	1.017 \pm 0.627	0.988 \pm 0.595
GeneZip-12.8K-AntiBioPrior	109.7 \pm 29.6	1.35 \pm 0.44	2.8548	0.6492	1.034 \pm 0.040	0.660 \pm 0.246	0.671 \pm 0.255
GeneZip-12.8K	766.5 \pm 2955.3	2.15 \pm 5.65	2.8660	0.4553	0.924 \pm 0.087	1.937 \pm 1.266	1.607 \pm 0.844
GeneZip-128K	774.4 \pm 2952.8	2.19 \pm 5.63	2.8351	0.3870	0.894 \pm 0.128	2.443 \pm 1.941	1.588 \pm 1.003

Results and discussion. Table 6 shows that on held-out chromosomes, the H-Net-BPT128 baseline substantially violates the intended token budget (BPT-ratio 11.50 ± 54.27), producing extremely long and highly variable tokens (Observed BPT 1664.9 ± 7943.4). In contrast, GeneZip models trained with the biological prior reduce this distribution-shift gap by roughly $5\times$, yielding BPT-ratio ≈ 2.2 while maintaining competitive perplexity.

Among GeneZip variants, length scaling to 128 Kbp yields the best language modeling quality (*GeneZip-128K*, PPL 2.8351) together with the strongest promoter enrichment (2.443 ± 1.941) and reduced intergenic enrichment (0.894 ± 0.128), indicating that the learned policy allocates more token budget to information-dense regulatory and genic sequence. It also achieves the lowest MicroErr (0.3870), and improves over *GeneZip-12.8K* (MicroErr 0.4553), indicating stronger adherence to region-level targets under distribution shift. At 12.8 Kbp, *GeneZip-12.8K* already achieves strong promoter/genic enrichment (1.937/1.607) but slightly worse perplexity (2.8660), suggesting that longer-context pretraining improves both LM quality and allocation sharpness. The *AntiBioPrior* ablation acts as a negative control: while it achieves a BPT-ratio closer to 1 (1.35 ± 0.44), it shifts token budget away from promoters and genic sequence (promoter/genic enrichment 0.660/0.671) and increases MicroErr (0.6492), showing that matching the *global* token count alone is insufficient; biologically grounded region supervision is necessary to steer allocation in a meaningful direction.

D. Enhancer-target Gene Prediction (ETGP) Experiments

We further assess whether GeneZip transfers to regulatory interaction prediction using the enhancer-target gene prediction (ETGP) task from DNALONGBENCH (Cheng et al., 2025). We fine-tune the GeneZip 12.8K checkpoint on the K562 dataset for 15 epochs with learning rate 1×10^{-3} . All other optimization and regularization settings follow the eQTL setup (AdamW, weight decay 0.1, $(\beta_1, \beta_2) = (0.9, 0.95)$, warmup ratio 0.1, gradient clipping at 1.0, BF16). We use per-device batch size 1 with gradient accumulation 8.

Table 7 reports AUROC and AUPRC. The Expert Model achieves the best AUROC (0.926), whereas GeneZip attains the best AUPRC (0.462), outperforming JanusDNA by

Table 7. AUROC and AUPRC for the enhancer-target gene prediction (ETGP) task. Higher is better. Best scores are in **bold**.

Model	AUROC	AUPRC
Expert Model(Cheng et al., 2025)	0.926	0.407
CNN(Cheng et al., 2025)	0.797	0.310
HyenaDNA(Cheng et al., 2025)	0.828	0.249
Caduceus-PH(Cheng et al., 2025)	0.826	0.380
Caduceus-PS(Cheng et al., 2025)	0.821	0.376
JanusDNA(Duan et al., 2025)	0.822	0.438
Ntv3-100M-pre(Boshar et al., 2025)	0.823	0.440
GeneZip	0.825	0.462

+0.024 (0.462 vs. 0.438) and the Expert Model by +0.055 (0.462 vs. 0.407). Although AUROC differences among neural baselines are small (e.g., 0.825 for GeneZip vs. 0.822 for JanusDNA), the AUPRC gain indicates that GeneZip yields a stronger ranking of enhancer–gene links among the top-scoring predictions. Overall, these results indicate that region-adaptive compression preserves regulatory signals that generalize beyond local variant-effect prediction to cross-element regulatory association.